ELSEVIER

Forest Biomass from Combined Ecosystem and Radar Backscatter Modeling

K. J. Ranson, G. Sun,† J. F. Weishampel,‡ and R. G. Knox**

Above-ground woody biomass is an important parameter for describing the function and productivity of forested ecosystems. Recent studies have demonstrated that synthetic aperture radar (SAR) can be used to estimate above-ground standing biomass. To date, these studies have relied on extensive ground-truth measurements to construct relationships between biomass and SAR backscatter. In this article we discuss the use of models to help develop a relationship between biomass and radar backscatter and compare the predictions with measurements. A gap-type forest succession model was used to simulate growth and development of a northern hardwood-boreal transitional forest typical of central Maine, USA. Model results of species, and bole diameter at breast height (dbh) of individual trees in a 900 m^2 stand were used to run discontinuous canopy backscatter models to determine radar backscatter coefficients for a wide range of simulated forest stands. Using model results, relationships of copolarized backscatter to forest biomass were developed and applied to an airborne SAR (AIRSAR) image over a forested area in Maine. A relationship derived totally from model results was found to underestimate biomass. Calibrating the modeled backscatter with limited AIRSAR backscatter measurements improved the biomass estimation when compared to field measurements. The approach of using a combination of forest succession and remote sensing models to develop algorithms for inferring forest attributes produced comparable results with techniques using only measurements. Applying the model derived algorithm to SAR imagery produced reasonable results when mapped biomass was limited to 15 kg/m^2 or less. ©Elsevier Science Inc., 1997.

* NASA / Goddard Space Flight Center, Biospheric Sciences Branch, Greenbelt

† Science Systems Application, Inc., Lanham, Maryland

‡ Department of Biology, University of Central Florida, Orlando, Florida

Address correspondence to K. J. Ranson, Code 923, NASA's GSFC, Greenbelt, MD 20771.

Received 17 November 1995; revised 7 May 1996.

INTRODUCTION

Recently, several studies have shown the capabilities of synthetic aperture radar for estimating forest structural parameters including above-ground biomass. Studies that have shown good correlations of backscatter and biomass for different forest stands include Dobson et al. (1992), LeToan et al. (1992), and Rignot et al. (1994). Generally the above studies found that longer wavelength cross-polarized radar backscatter was the most sensitive to woody biomass. Ranson and Sun (1994) and Ranson et al. (1995a) used combinations of longer (i.e., P- or L-band) and shorter wavelength (C-band) airborne and satellite SAR data to map above-ground woody biomass in northern forests in Maine and Canada, respectively. Dobson et al. (1995) used forest type classification and radar channel combinations to develop relationships between SIRC / XSAR backscatter and several different forest attributes, including biomass and tree height, in a Michigan, USA forest. All of these studies required the collection of extensive ground truth measurements from which to derive the appropriate biomass and radar backscatter relationship or algorithm. Field measurements are vital to any careful study, but it is often extremely difficult and expensive to acquire sufficient measurements to characterize the full range of forest conditions, especially in remote and structurally diverse forests.

An alternative to relying exclusively on field measurements for algorithm development is using radar backscatter models to help develop relationships between radar data and forest parameters. Backscatter modeling of forest canopies has received much attention over the past decade with numerous investigators reporting progress on backscatter modeling of forest stands. A number of radar backscatter models (e.g., Richards et al., 1987; Ulaby et al., 1990; Durden et al., 1989; Chauhan et al., 1991; Lang et al., 1994) have been developed for various kind of forests. These models treat the forest canopy as a horizontally homogeneous medium. For modeling forest stands of low to medium den-

REMOTE SENS. ENVIRON. 59:118–133 (1997)

655 Avenue of the Americas, New York, NY 10010

0034-4257 / 97 / $17.00
PII S0034-4257(96)00114-9

sities, discontinuous radar backscatter models have been developed, treating each tree as an individual scatterer (Sun et al., 1991; McDonald and Ulaby, 1993; Wang et al., 1993; Whitt and Ulaby, 1994). A three-dimensional radar backscatter model was developed by Sun and Ranson (1995) for investigating effects of forest spatial structure on radar backscattering. These and other models have been used to simulate radar backscattering from various forest stands, but few attempts have been made to use the models to develop algorithms for extraction of forest biophysical attributes from SAR data.

Pierce et al. (1994) presented results of inversion of modeled backscattering of aspen stands of different ages by using an artificial neural network. The inputs to the network included incidence angle and HH, VV, and HV backscattering at L- and C-bands, and ratios of LHH/CHH, LVV/CVV, and LHV/CHV. A total of 55 stands were modeled for training the network and testing the inversion. Polatin et al. (1994) developed a general model-based iterative algorithm for use in the inversion of polarimetric radar data. The results of estimation of four canopy parameters, that is, soil moisture, trunk canopy density, trunk height, and leaf canopy density, utilizing four radar data channels (LHH, LVV, CHH, and CVV) were presented. In both studies the radar data were simulated with the radiative transfer model (MIMICS) of Ulaby et al. (1990) and used as input to the algorithms. However, the algorithms were not applied to actual SAR data. In a study by Saatchi and Moghaddam (1994), a hybrid technique of image classification, modeling, and inversion was developed for extracting vegetation biomass from SAR data. Their methodology relies on an accurate land cover map and a physically based vegetation backscatter model parameterized by field measurements.

Another approach is to use forest succession models to provide inputs to radar backscatter models. Kasischke and Christensen (1990) outlined, in general terms, steps to connect forest ecosystm models with radar backscatter models. They suggested the use of forest growth models to help develop and validate backscatter models that predict the radar signature based on tree stand characteristcs. The objective of their proposed technique was to provide inputs to forest models. Ranson et al. (1994) demonstrated that radar backscatter models can be parameterized using a forest succession model and that the results closely followed observed trends. Optical and microwave models have been used to develop algorithms for leaf area index and biomass, respectively (Smith et al., 1994; Ranson et al., 1995b).

In this article, we expand upon the work of Ranson et al. (1994; Ranson et al. 1995b) and demonstrate that a forest growth model can be used to parameterize and exercise a radar backscatter model with the goal of developing algorithms for inferring forest attributes from SAR imagery. Figure 1 is a diagram of the approach followed here. First a forest model is run for a range of conditions over 250 years. The resulting stand parameters are then input to a radar backscatter model and backscatter coefficients (σ°) are simulated. The σ° and forest model simulated biomass are used to develop a relationship or algorithm for estimating biomass from radar backscatter. Using calibrated σ° enables the testing of model results with field measurements and SAR image data. The resulting backscatter and modeled forest biomass are used to examine the relationships between individual and combinations of radar channels. In the following sections, we describe briefly our study area and data acquisition. Some background information about forest ecosystem models is presented, and the approach and results from the modeling analyses are described. Finally, a discussion of the model results and validation using SAR imagery is presented.

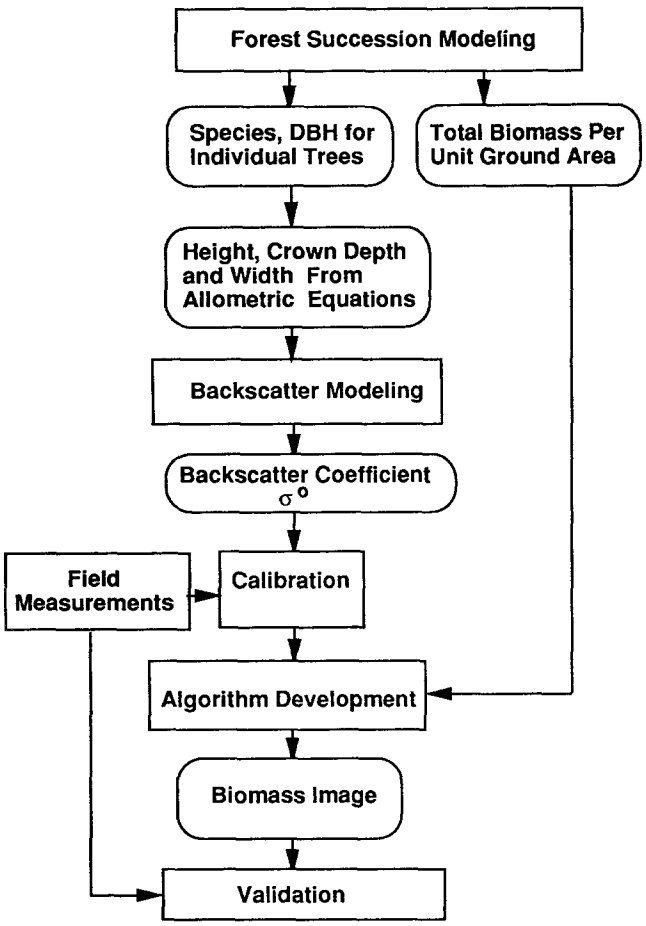

Figure 1. Diagram of combined modeling approach.

STUDY SITE AND DATA

The combined modeling work discussed in this article was conducted for forest types found at International Pa-

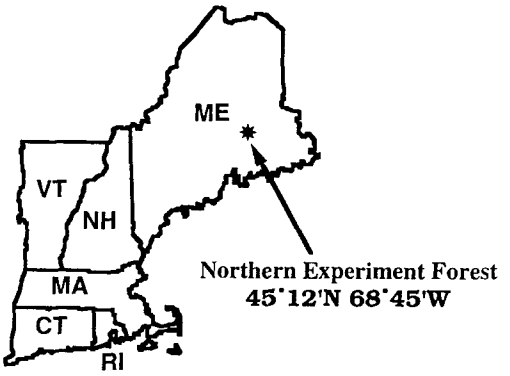

Figure 2. Location of the Northern Experimental Forest is near Howland, Maine, USA.

per's Northern Experimental Forest (NEF). This study site is located near Howland, Maine USA (45° 12′N, 68° 45′W) (Fig. 2). The NEF is representative of a boreal-northern hardwood transitional forest consisting of aspen–birch, hemlock–spruce–fir, and hemlock–hardwood mixtures. The 10 km×10 km study area consists of large tracts of unmanaged forest stands, small plantations, and naturally regenerating clearings of various ages. Because the management programs are often experimental, useful historical data on specific areas are available. Topographically, the region varies from flat to gently rolling, with a maximum elevation change of less than 135 m. Due to the region's glacial history, soil drainage classes within a small area may vary widely, from excessively drained to very poorly drained. Nearly 450 ha of the central NEF consists of bogs and other wetlands. Consequently, a patchwork of forest communities has developed, supporting exceptional local species diversity. Generally, the soils throughout the forest are glacial tills, acid in reaction, with low fertility and high organic composition. The climate is mostly cold, humid, and continental with mean annual precipitation of about 900 mm and a snow pack accumulation of up to 2 m from December through March. This site was the focus of a NASA Multi-sensor Aircraft Campaign (MAC) for the Forest Ecosystem Dynamics project at GSFC (e.g., Goward et al., 1994) and was a backup Supersite for the recent SIR-C/XSAR missions.

Attributes of several forest stands within the study area were sampled during 1992 and 1994. Candidate sites were identified from aerial photography and SAR imagery and located by distance and bearing from obvious landmarks. The sites were visited by field teams who identified tree species and measured the diameter breast height (dbh) for all trees within three to five 4-m-radius fixed-area plots. Because of the variability of soil types across the study area, forest stands of homogeneous cover (i.e., species composition, height and density) are relatively small. Average coefficient of variation (Standard deviation/mean·100%) among sample plot biomass measurements was about 40%, which indicates that the forest stands have much variability. These data are described in more detail in Ranson and Sun (1996). Biomass was calculated from dbh measurements using weight tables for Central Maine forests published by Young et al. (1980). Figure 3a presents a histogram of species weighted by biomass density. Figure 3b shows the distribution of measured stands in terms of the percent composition deciduous (broad leaf) and coniferous (needle leaf) species. These data show that over 60% of the biomass in the study areas is attributed to conifer species with hemlock accounting for nearly half of that total (Fig. 3a). The data presented in Figure 3b show that conifer species were dominant in about 65% of the stands with about 22% in roughly even mixtures and only 13% dominated by deciduous species. Of the seven

Figure 3. Forest composition of the NEF: a) histogram of species recorded for sample plots; b) distribution of measured stands as percent needle leaf (conifer) and broadleaf (deciduous). Species codes are: PIRE—red spruce, TSCA—eastern hemlock, THOC—northern white cedar, PISP—white pine+red pine+jack pine, ABBA—balsam fir, ACRU—red maple, POSP—aspen, BESP—birch, FAGR—American beech, MISC—green ash+alder+willow.

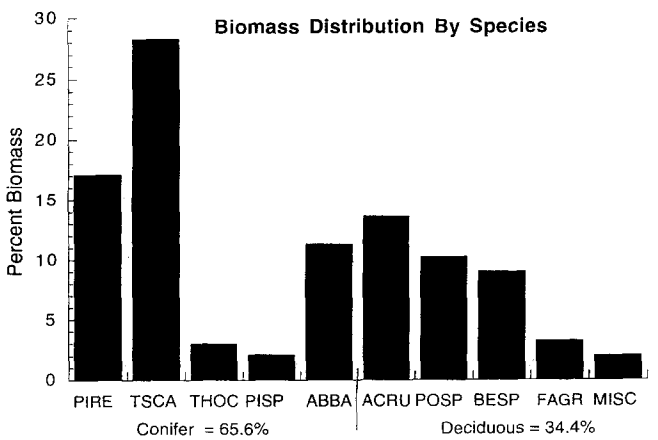

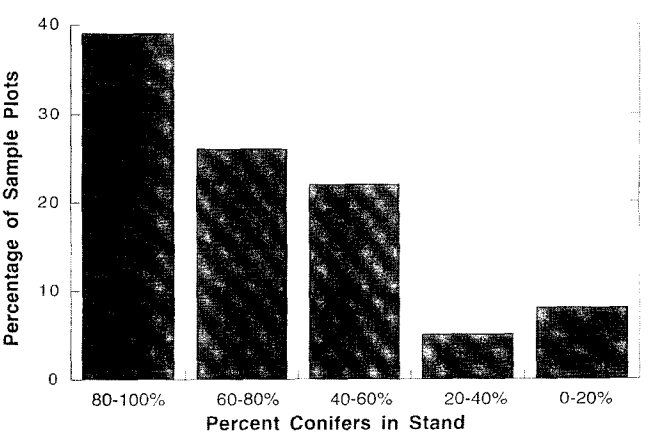

stands in the deciduous category three were regenerating clear cuts with very low biomass, leaving four stands with biomass ranging from about 4 kg/m^2 to 21 kg/m^2. For this reason this work does not consider differences in forest structure in the development of the biomass algorithm discussed below.

The JPL airborne synthetic aperture radar (AIRSAR) was flown aboard the NASA Ames DC-8 on 9 June 1991 with P-, L-, and C-band frequencies and polarizations of HH, VV, HV, and VH. Radar data was collected for three image center incidence angles (25°, 35°, 45°) while looking north over the Northern Experimental Forest test area. By flying a "race track" trajectory, two southerly looking views were also obtained (35° and 50° incidence). Preceding the overflights, field personnel positioned five trihedral corner reflectors inside the study site for SAR image calibration. An image with center incidence angle of 35° looking toward the north (actual flight heading was 72°) is used for this study.

The data was received from JPL in compressed Stokes matrix format with 4 looks and a resulting ground range resolution of 12.2 m. The data was calibrated using routine procedures outlined in POLCAL (van Zyl et al., 1990), using the corner reflectors. The radar incidence angles varied from 34.8° to 45.7° across the portion of the image occupied by the stands. The image data was displayed to determine the locations of each measured stand. A 5×5 block of pixels for each radar channel was extracted from the center of the stands using Image Processing Workbench routines (Frew, 1990). The relatively small number of pixels was used to ensure that the signatures were extracted from within the measured forest stands. The average backscatter from a site was used later for calibration and field checking of the model results.

FOREST MODELING

Mathematical models that simulate forest dynamics have gained widespread acceptance and use over the past 2 decades. The most successful models (in terms of general applicability to diverse forest types) are individual tree-based models called gap models (Shugart et al., 1992; Botkin, 1993). For example, these models have been used to simulate tropical rain forest (Doyle, 1981) to boreal forest (Bonan et al., 1990) dynamics and the effects of different disturbance regimes, for example, fire (Shugart et al., 1980), flooding (Pearlstein et al., 1985), and hurricane (Doyle, 1981) as well as the effects of past (Bonan and Hayden, 1990) and potential (Pastor and Post, 1988) climate change on forest structure and composition. Although this class of models has been used to predict changes in growth rates associated with changes in abiotic factors, this ability is largely untested (Hinckley et al., 1994). The strength of these models lies in their versatility to predict qualitative successional patterns related to species composition and forest structure.

Although these models differ to a certain degree depending on the denizen species, the ambient environment, and the objectives of the study, they all possess certain similar key features. The majority of gap models simulate the dynamics of a forest by computing the birth, growth, and death of individual trees in response to environmental conditions found on a plot with roughly the projected area of a dominant crown (i.e., 0.01–0.1 ha) or gap which forms when such a tree dies. Growth of individuals is deterministic based on species-specific functions that relate potential diameter increment to current size. This potential increment is reduced according to the constraints of the site conditions (e.g., temperature, available light, soil moisture, and soil fertility), which, in some cases (e.g., available light) are dependent on the structure of the trees inhabiting the plot. Birth and mortality, however, are stochastic. Relative sapling establishment probabilities for each species are constrained by the ambient conditions (e.g., available soil moisture and light reaching the ground). Likelihood of mortality is determined from the maximum expected longevity of each species and is increased for individuals failing to achieve minimal growth (e.g., those suppressed by shading). The dynamics of a forest stand are determined as the summation of the dynamics of the individual trees. Thus, these models permit the simultaneous consideration of individual- and population-level phenomena. This approach allows inclusion of information collected at the individual tree level (e.g., physiologic processes, species silvics, and specific attributes of particular trees at different ages and sizes) to enable stand level predictions. Results detailing populations of simulated individuals can then be used directly to represent intrinsic variation within and among forest stands. In addition, these data can be aggregated into stand attributes such as tree density or biomass density. This class of forest models is well established as suitable for reproducing forest community dynamics to use in other applications, most commonly models of nutrient cycling. Their primary limitations are in representation of controlling mechanisms underlying this behavior (see Pacala et al., 1996). In this article the forest model is used as a structural simulator for a range of ages and soil conditions.

Forest Model Implementation

The forest model ZELIG (Urban, 1990), adapted as described in Levine et al. (1993), was used to simulate the successional dynamics of the southern boreal/northern hardwood forest transition zone found at the NEF. Because soil moisture is considered to be of primary importance in determining the structure (e.g., biomass and species composition) of the forests (Bonan and Shugart, 1989), waterlogging effects [adapted from Botkin (1993)] were included. This required connecting the ZELIG model to a soil physics model that simulates depth to saturated soils (see Weishampel et al., 1996).

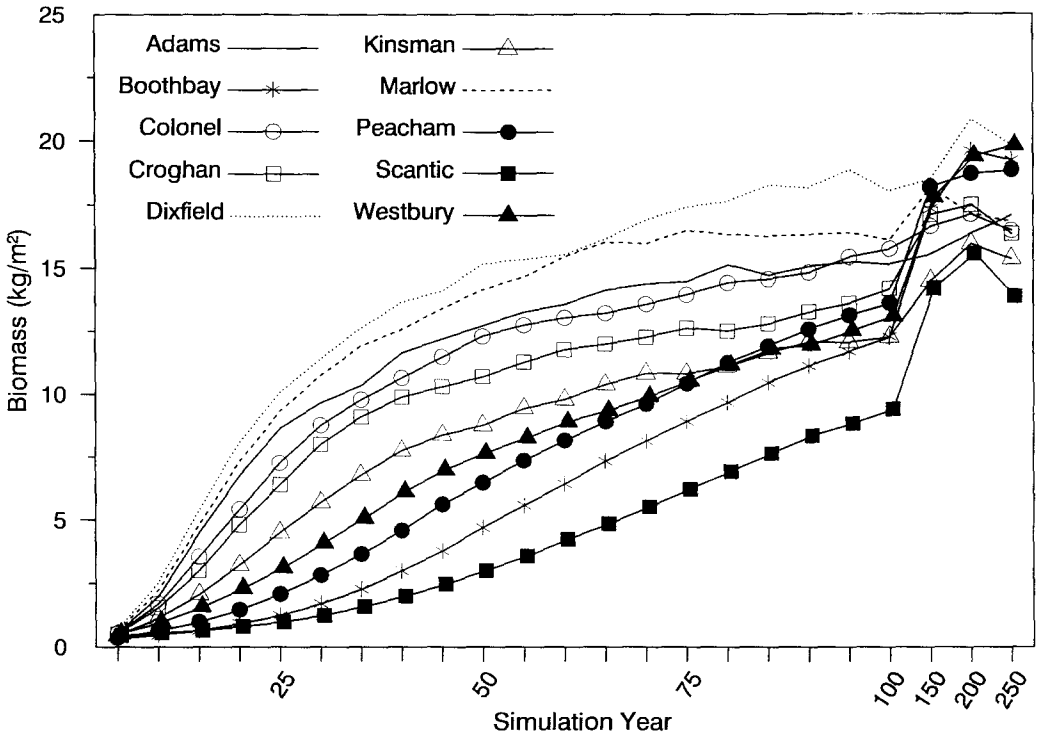

Figure 4. Results of forest model simulations of average biomass for 10 different soils over a time period of 250 years.

To implement the model, site parameters (e.g., soil fertility and monthly values of temperature and precipitation) and autecological parameters (e.g., height and diameter maxima and growth tolerances) were derived from empirical data and published sources (e.g., Pastor and Post, 1985; Botkin, 1993). Forest succession on ten soil types (see Table 3) found at the NEF were simulated starting from bare ground. Depth to water saturated soil and water holding capacity of the soil were derived using a soils process model (Levine et al., 1995). The spatial scale of the ZELIG simulations were performed at a resolution (30×30 m) to correspond to the scale of typical remotely sensed data. To do this, model-generated structural attributes [e.g., diameter at breast height (dbh), height, height to base of crown, and foliage density] were recorded for each individual tree in nine (10 m×10 m) ZELIG plots. Model results were recorded at 5-year intervals up to 100 years and at 50-year intervals over 250 years. Because gap models possess underlying stochasticity in their regeneration, mortality, and weather routines, 15 separate runs were performed to generate a range of stand responses. Figure 4 shows the average biomass trajectories simulated for 15 30 m×30 m (900 m^2) stands growing on the 10 NEF soil types over the 250-year simulation. The range of biomass simulations illustrate the importance of considering soil types in our study area. Generally, better drained or mesic soils produced higher biomass values whereas poorly drained and wet soils produced lower biomass values (see Table 3). Because of the stochastic timing of tree birth and death, replicate simulation can exhibit considerable variation about these averages. The simulated biomass trends and the underlying patterns of dominance by needle leaf (conifer) and broadleaf (deciduous) species were consistent with field measurements reported by Ranson and Sun (1994) and Levine et al. (1994). A total of 3450 simulations were rerecorded for use with the radar model (10 soil types×15 replications×23 time steps). The simulation results were used to provide input information to a radar backscatter model as discussed below.

BACKSCATTER MODELING

A discontinuous radar backscatter model described by Sun et al. (1991) was used in this study. In a discontinuous forest stand, a radar beam can interact with forest stands in three ways: 1) intersecting at least one tree crown; 2) intersecting no trees—that is, incident directly on the ground surface through gaps between trees and producing a direct surface backscattering; and 3) encountering a tree trunk and giving a strong forward scattering involving trunk–ground interaction, especially if the surface is relatively smooth and wet. Tree crowns were modeled as ellipsoids consisting of a mixture of leaves and branches with various sizes and orientations. Trees were assumed to be randomly positioned in a stand with

the distribution of tree size assumed to be log-normal. Inspection of ZELIG model simulations showed that distributions of simulated heights approximated log-normal, especially for stands 30–100 years in age. With these assumptions, a simpler formula can be used to estimate the probabilities of a radar beam passing through gaps or intersecting with the tree crowns (Sun et al., 1991). Radar backscattering and attenuation resulting from interactions within the forest canopy were dependent on these probabilities. These components are considered to have independent phases so that the Stokes matrices of these components may be added together to obtain the Stokes matrix of total backscattering of the forest stand.

Backscatter Model Implementation

The radar backscatter model was parameterized with the stand structural attributes generated from the forest succession model discussed above. Forest model output parameters include species, dbh, total height, and trunk height for every tree growing on a simulated plot. The backscatter model requires dbh, trunk height, total tree height, crown half-width and half-height, and branch and

Table 1. Measured Forest Parameters Used by Backscatter Model for Broad Leafed and Needle Leafed Trees

Parameter	*Broadleaf*			*Needle Leaf*		
			Crown[a]			
Half-width	r=0.09592∘h			r=0.15607∘h		
Half-height	b=0.22517∘h			b=0.27813∘h		
			Branch[b]			
Orientation Angles	*Angle (deg)*		*Probability*	*Angle (deg)*		*Probability*
	0–10		0.01	0–10		0.015
	10–20		0.01	10–20		0.02
	20–30		0.08	20–30		0.015
	30–40		0.23	30–40		0.03
	40–50		0.30	40–50		0.14
	50–60		0.19	50–60		0.25
	60–70		0.11	60–70		0.22
	70–80		0.06	70–80		0.14
	80–90		0.01	80–90		0.17
Branch Size[c] *Distribution*	*Diameter (cm)*	*Length (cm)*	*Probability*	*Diameter (cm)*	*Length (cm)*	*Probability*
	0.5	7.5	0.68	0.2	15	0.86684
	1.5	22.5	0.15	0.4	30	0.10312
	3.5	52.5	0.10	0.6	40	0.01605
	6.0	90.0	0.05	0.8	75	0.00619
	9.0	135.0	0.02	1.1	90	0.00481
				2.4	165	0.00154
				3.0	260	0.00119
				3.5	350	0.00025
Number of branches (m^3)		20			105	
			Leaf			
Width (cm)		6.4			0.08	
Length (cm)		6.4			0.8	
Thickness (cm)		0.1			0.8	
Density, leaves (m^3)		400			196,000	
Orientation		Planophile (assumed)			Planophile[d]	

[a] Crown shapes are ellipsoidal. Equations for r and b from Strahler (1995). h=canopy height from forest model.

[b] Branch orientation angles for broadleaf and needle leaf canopies derived from Hall et al. (1992).

[c] Branch size distribution from Hall et al. (1992). The ratio of length to diameter was assumed to be 15 for all branches. Needle leaf branch size distribution from Chauhan et al. (1991).

[d] Leaf angle from normal to leaf surface from Kimes and Smith (1991).

Table 2. Real and Imaginary Dialectic Constants for Tree Components for Backscatter Modeling

	Broadleaf		*Needle Leaf*	
	Foliage	*Wood*	*Foliage*	*Wood*
C-band	19.2, 6.61	11.68, 4.03	17.62, 6.08	13.64, 4.72
L-band	23.23, 7.68	14.67, 5.07	21.45, 7.16	16.96, 5.81
P-band	26.49, 13.11	17.37, 7.95	24.61, 12.06	19.88, 9.32

foliage parameters (i.e., size and orientation distributions of leaves and branches).

Diameter breast height (dbh) from the forest model was used directly by the radar model. Although total tree height and trunk height were available from the forest model, they were calculated within the radar model from dbh and allometric relationships developed from field measurements. Crown half-width and half-height were calculated as a function of calculated tree height and species type provided from the forest model (Table 1). Branch and foliage parameters were determined and assigned based on forest model species type (i.e., broadleaf and needle leaf) from data reported by Chauhan et al. (1991) for hemlock (needle leaf) and Hall et al. (1992) for aspen (broadleaf). Needle orientation distributions used were based on the work of Kimes and Smith (1991) for hemlock and closely followed a planophile (mostly horizontal leaves). The distribution of broadleaf angles was assumed to be planophile.

Surface backscattering was calculated by use of the IEM model (Fung and Pan, 1987) and the surface roughness was specified by an RMS height of 1 cm and a Gaussian correlation function with correlation length of 6 cm. Different surface soil moisture contents and dielectric constants were estimated for 10 representative soil types found in the study area based on published soil characteristics (USDA, 1990; Levine et al., 1994) and field measurements. The dielectric constants at C- and L-bands were calculated from soil texture and moisture using equations given by Hallikainen et al. (1985). Table 3 gives the dielectric constants used for the 10 soil types. Since the empirical models of Hallikainen et al. do not cover the frequency at P-band, the dielectric constants for P-band listed in Table 3 were assumed based on those at C- and L-bands.

The backscatter model also requires dielectric constants for wood, foliage, and the ground surface. Dielectric constants of woody and foliage components listed in Table 2 were calculated from air temperature, dry material density (Wenger, 1983), and measured volumetric moisture contents using the dual-dispersion model described by Ulaby and El-Rayes (1987). The moisture contents for tree components were assumed not to vary as a function of soil type.

All radar model simulations were run with an incidence angle of 40°. This angle was chosen because it is in the middle of the range of image incidence angles (34.8° to 45.6) for the measured forest stands. Backscattering coefficients of HH, HV, and VV polarizations at P-, L- and C-bands were simulated for the 3450 stands. Since the discontinuous model used in this study is a first-order solution of the radiative transfer equation, the cross-polarization returns tend to be underestimated, especially at shorter wavelengths (Karam et al., 1994). The copolarized radar channels also produce higher backscatter levels and can be more accurately calibrated, so that only copolarized data were used in this study. The use of copolarized backscatter is a limitation in the applicability of this procedure since it is well known that cross-polarized backscatter is more sensitive to forest biomass (e.g., Dobson et al., 1992; LeToan, 1992; Ranson and Sun, 1994). However, the purpose here is to demon-

Table 3. Soil Moisture, Soil Texture, and Dielectric Constants (Real, Imaginary) Used in the Forest and Backscatter Modeling

	Texture			*Dielectric Constants Real, Imaginary*		
Series	*% Water*	*% Clay*	*% Sand*	*C-Band*	*L-Band*	*P-Band*
Adams	9.6	6.3	66.6	5.34, 0.65	6.02, 0.90	6.60, 1.20
Boothbay	28.1	20.0	16.6	13.53, 2.85	13.72, 3.81	14.20, 3.60
Colonel	24.2	3.0	56.1	13.56, 2.70	14.60, 2.14	15.80, 2.50
Croghan	6.7	1.4	78.8	4.26, 0.40	4.97, 0.68	5.50, 0.80
Dixfield	17.0	2.8	59	9.14, 1.54	9.92, 1.53	10.50, 1.80
Kinsman	10.6	1.9	80.1	5.87, 0.77	7.05, 0.98	8.00, 1.50
Marlow	19.70	3.7	48.2	10.50, 1.86	10.95, 1.82	11.50, 1.70
Peacham	21.8	5.1	51.5	11.72, 2.22	12.44, 1.98	12.80, 1.60
Scantic	39.4	33.2	12.5	20.28, 5.27	22.77, 5.61	24.00, 6.20
Westbury	15.3	4.4	59.8	8.15, 1.31	8.90, 1.39	9.20, 1.42

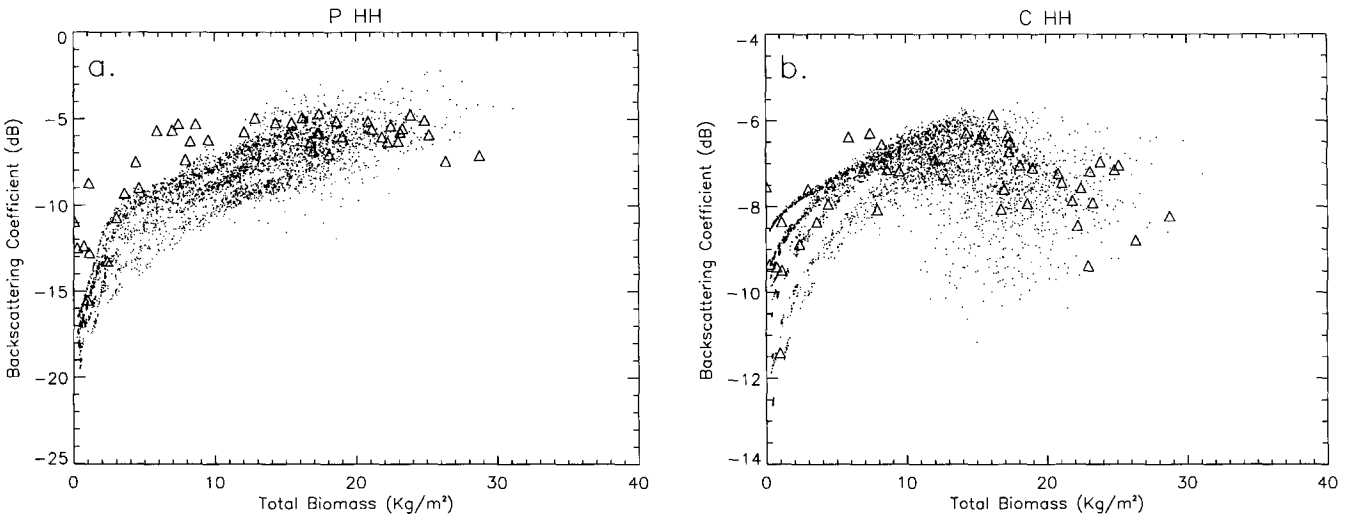

a b

Figure 5. Simulated PHH (a) and CHH (b) backscattering versus total dry above-ground biomass for 3450 modeled forest stands (dots). Triangles represent measured SAR backscatter and above-ground dry woody biomass for 46 measured stands.

strate the feasibility of using forest growth models with radar backscatter model that can be satisfied with the use of copolarized backscatter. Figure 5 shows the simulated PHH and CHH backscattering versus total dry above-ground biomass. When the total biomass is low, the radar beam impinges the forest floor so that the return is more dependent on soil moisture. This effect can be seen as separate curves at low biomass especially at C-band (Fig. 5b). According to the model results, drier soils will have lower backscatter. After total biomass exceeds about 10 kg/m^2, C-band backscattering is dominated by tree crowns so the influence of soil moisture is reduced. At P-band, however, the effect of soil moisture remains visible until total biomass reaches about 15 kg/m^2 because of the trunk–ground double-bounce backscattering. AIRSAR signatures of 46 field-sampled stands extracted from an image of 9 June 1991 were also plotted with triangles in Figure 5. From Figure 5a it is seen the PHH SAR observations are 3–5 dB higher than the model results at lower biomass levels. It also appears the modeled backscatter is more sensitive to biomass over a greater range than the SAR data. Since the measured stands represent a wide range of ground conditions (roughness and moisture), species composition, and forest spatial structures the differences between simulated and SAR backscattering show that the modeling process was not able to simulate all of these conditions. However, the forest model runs produced stands with a greater variety of forest composition and biomass than were measured. In addition, the model output reduces the backscatter modeling effort to consider those forest attributes of species, tree size and combinations of biomass, leaf area, height, and density that are realistic for typical forests of central Maine, USA.

ALGORITHM DEVELOPMENT

Algorithm from Simulations

The first step in the algorithm development process was to examine the relationships of modeled backscatter to the modeled biomass. A stepwise analysis using the STEP function in the S-Plus[1] (MathSoft, 1993)[1] software package was used to provide an automated procedure for selecting the best linear regression model by adding and dropping independent variables. Six backscattering coefficients (i.e., HH and VV at P, L- and C-bands) were used as independent variables. Both the cube root of total biomass and the logarithm of total biomass were examined as dependent variable. The logarithm form was tested since it has been found to provide good biomass relationships with radar data (e.g., Le Toan et al., 1992). The cube root of biomass was also tested since the cube root transformation equalized the variance and produced a normal distribution of the biomass data. From a physical standpoint, woody biomass is related to woody volume, the cube root of which represents a characteristic linear dimension for that volume.

The model selected as the best of all single multichannel combination was the cube root of total biomass with backscatter (dB) from four radar channels:

$$B^{1/3} = 1.9085 + 0.1909\ \mathrm{PHH} - 0.6815\ \mathrm{CHH} + 0.4516\ \mathrm{CVV} - 0.0116\ \mathrm{PVV}, \quad R2 = 0.95. \quad (1)$$

The reason for the form of the above model is not very intuitive, but Eq. (1) can be simplified by dropping the PVV term since the coefficient is very close to zero.

[1]Use of trade names are for information only and do not imply endorsement by the U.S. Federal Government.

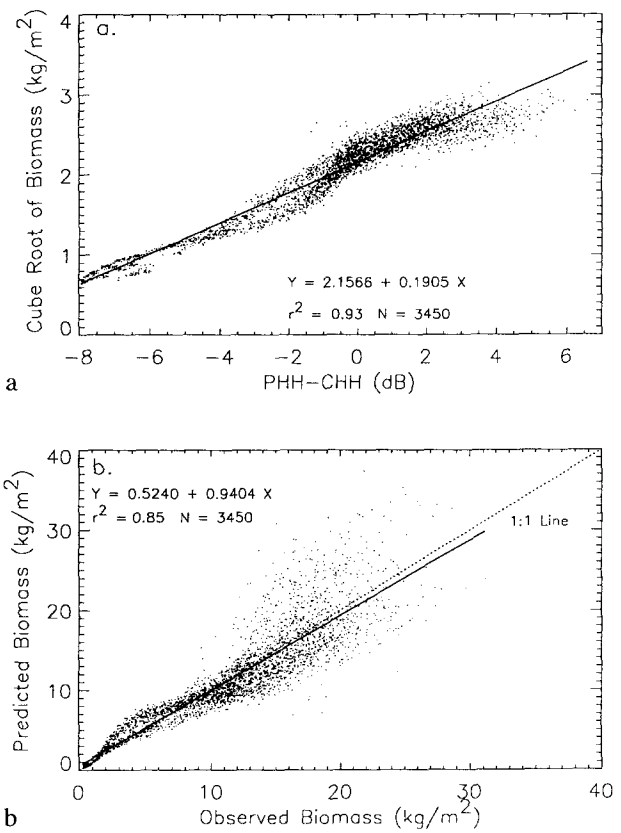

Figure 6. a) Relationship between cube root of biomass estimated with forest model and PHH-CHH from the backscatter model for 3450 simulated stands. b) Comparison of biomass determined from linear model shown in a) and forest model biomass.

Since CHH and CVV backscatter are nearly equal for forested areas, the CVV coefficient can be subtracted from the CHH coefficient leaving

$$B^{1/3}=1.909+0.1909\ \mathrm{PHH}-0.2299\ \mathrm{CHH}.$$

This leaves an equation with similar coefficient for the two variables so a new regression was conducted using only PHH and CHH data. The resulting regression equation was

$$B^{1/3}=2.2296+0.1894\ \mathrm{PHH}-0.1810\ \mathrm{CHH}, \qquad r^2=0.94.$$

A final regression analysis was performed with a simple linear form of the relationship with the independent variable expressed as (PHH−CHH), which is the logarithmic form of the ratio of PHH to CHH. A new biomass regression equation was developed using PHH−CHH, calculated from the modeled backscatter, as the independent variable:

$$B^{1/3}=2.1566+0.1905\ (\mathrm{PHH}-\mathrm{CHH}), \qquad r^2=0.93. \quad (2)$$

This simple relationship appears to be equivalent to Eq. (1) with only a small decrease in r^2. Figure 6a shows the regression relationship (solid line) between $B^{1/3}$ and PHH–CHH for the 3450 simulated stands plotted with the backscatter model results (dots). Note the effects of soil moisture observed in Figures 5a and 5b have been reduced by the use of the band combination. Comparing predictions of estimated biomass using Eq. (2) with forest model predicted biomass produced an r^2 of 0.85 and residual standard error of 2.60 kg/m^2.

Algorithm from SAR Data And Field Biomass Measurements

A stepwise analysis was also performed with the measured biomass and AIRSAR backscatter data from 46 stands and again the PHH/CHH combination was found to be the best, keeping in mind that only copolarization data was considered. The resulting equation was

$$B^{1/3}=2.581+0.315\cdot\mathrm{PHH}-0.249\ \mathrm{CHH}, \qquad R^2=0.71. \quad (3)$$

Analyzing the measured biomass and combined backscatter data (PHH–CHH) yielded a relationship similar to Eq. (2):

$$B^{1/3}=2.117+0.324\cdot(\mathrm{PHH}-\mathrm{CHH}), \qquad r^2=0.74. \quad (4)$$

Figure 7a is a plot of the field measured biomass and PHH-CHH backscatter obtained from AIRSAR. Figure 7b is the biomass estimated from the AIRSAR data and Eq. (4) and indicates that biomass is being overestimated for low levels, but underestimated for higher levels using Eq. (4). Comparing Figures 6a and 7a, it can be seen that the intercept terms are similar, but the slope of the equation derived from modeling results [Eq. (2)] is lower. Modeled backscatter values also have a greater range than AIRSAR backscatter. For both cases there is much variation from the best-fit line, which is a product of the wide variety of measured and modeled forest conditions.

It is apparent from Figures 5 and 6 that the backscatter model does not adequately simulate the backscatter in all cases. For example, the AIRSAR data were up to 5 dB higher for biomass less than 10 kg/m^2, but actually fell below the simulated values at higher biomass levels. CHH simulations, on the other hand, fit the measured AIRSAR data much better. Examining Figures 6 and 7, it appears that the backscatter model produces PHH backscatter with a greater range than that observed in the AIRSAR data for forest stands. The result will be a greater range in PHH-CHH and the smaller slope observed in Eq. (2). We believe this is the result of the ground surface characteristics used for the modeling not adequately characterizing the wide variety of surface roughness conditions found in the study area. Additional variation may be due to radar parameters not accounted for in the model. Thus, it was decided to attempt a calibration of the modeled backscatter to produce a better fit with the AIRSAR measurements.

Algorithm from Calibrated Model Results

We assumed that the systematic errors due to effects of radar parameters or scene conditions not accounted for

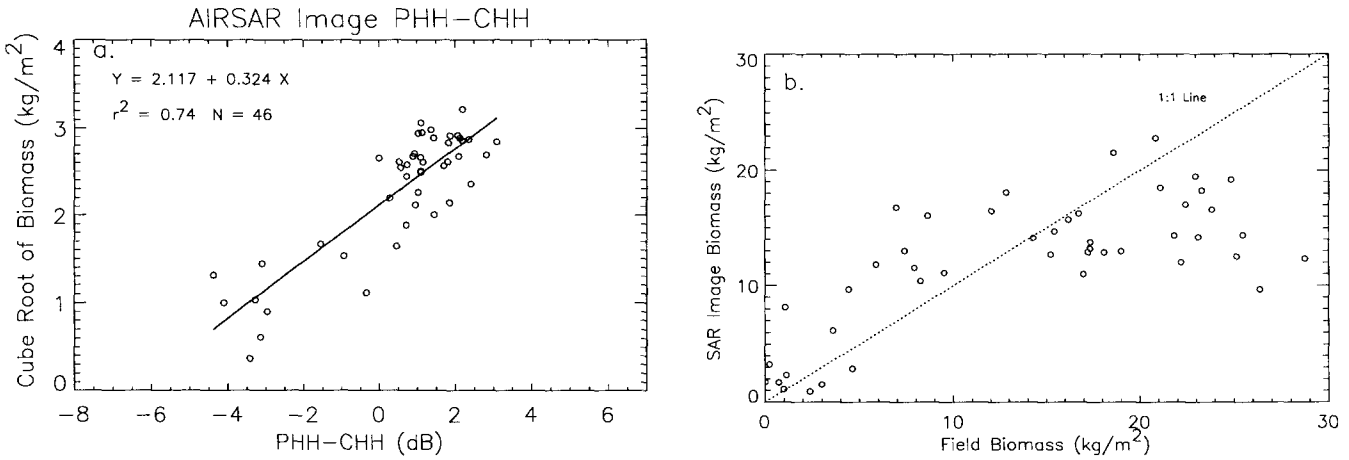

a b

Figure 7. a) Relationship of the cube root of field measured biomass ($B^{1/3}$) and PHH-CHH backscatter from AIRSAR image. b) Comparison of biomass determined from linear model shown in a) and field measured biomass.

in the modeling could be corrected by using AIRSAR backscatter from measured stands with similar attributes to modeled stands. The modeling data set was examined, and 19 stands were identified that were similar to field-sampled stands in terms of stem density, total biomass, and conifer / deciduous composition (Table 4). The backscattering coefficients from the AIRSAR image were extracted and compared with the modeled backscatter. The simulated PHH and CHH backscattering coefficients were calibrated with the regression equations for PHH and CHH data, and a new algorithm was developed:

$$B^{1/3}=2.0505+0.2627*(\text{PHH–CHH}), \quad r^2=0.83. \quad (5)$$

The intercept of Eq. (5) is very close to the that derived from the field data [see Eq. (4)]. There was also some improvement in the slope from that observed in Eq. (2), which brings the range of the modeled backscatter into closer agreement with the measurements.

ALGORITHM VALIDATION AND BIOMASS MAPPING

One objective of this research was to determine if radar backscatter and forest ecosystem modeling could be used to provide insight into what relationship to use for esti-

Table 4. Summary of Measured and Modeled Stand Parameters for Stands Used To Calibrate Modeled Backscatter Data

	Density (trees / ha)		*Biomass (kg / m^2)*		*% Needle Leaf*	
Site	*Field*	*Model*	*Field*	*Model*	*Field*	*Model*
2	663	2244	0.23	0.26	93.4	49.5
8	7148	5678	4.63	4.68	71.3	84.8
11	1916	4344	0.88	0.88	89.7	77.9
12	884	4589	0.77	0.77	100.0	70.4
13	1989	4300	1.08	1.07	96.9	77.9
15	2506	4500	5.89	5.84	85.8	94.0
21	2210	4144	7.42	7.45	97.0	93.1
24	2727	2411	20.79	20.57	37.9	35.6
25	3831	3322	15.25	14.22	91.2	85.2
28	3684	3344	12.95	12.91	60.5	54.3
31	3021	7622	8.63	8.63	17.3	25.3
32	2431	2333	18.84	18.89	83.1	80.0
33	4127	3511	18.63	18.43	58.6	58.3
36	2431	2100	16.99	17.0	47.3	44.6
40	1548	1433	28.77	27.51	53.2	50.6
43	2358	5322	10.80	10.83	47.7	35.6
44	5231	4556	14.21	14.23	86.3	56.0
55	3389	3333	8.25	8.23	79.1	97.1
58	2800	2500	12.82	12.94	79.6	80.3

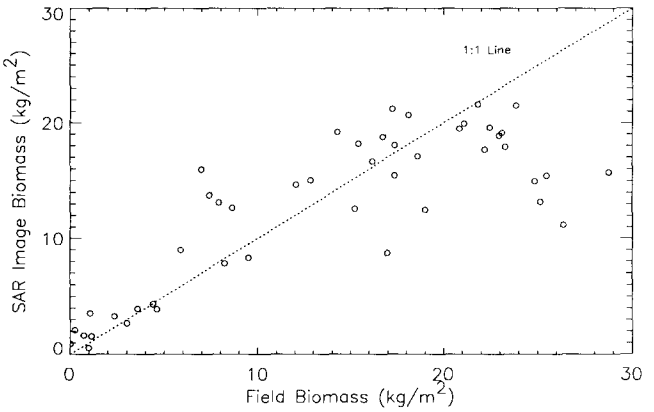

Figure 8. Biomass estimated with PHV-CHV AIRSAR backscatter using algorithm reported by Ranson and Sun (1994) plotted with field measurements.

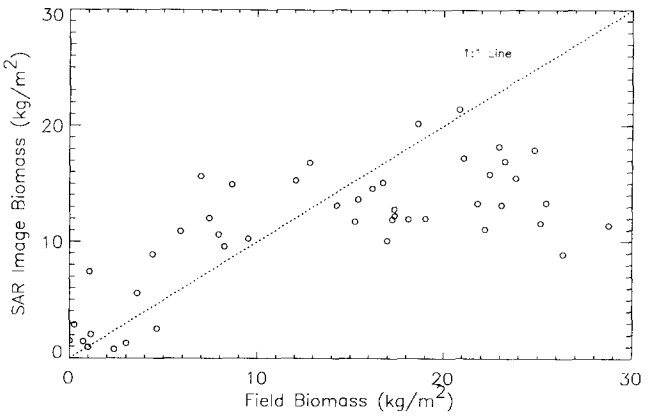

Figure 9. Biomass predicted using calibrated model backscatter [Eq. (5)] plotted with biomass observed from field measurements.

mating forest biomass from radar backscatter. This was accomplished above by demonstrating similar results in model selection using both modeling and measurements. The calibration of the model backscatter using a few stands provides the opportunity to go a step farther and investigate if the model generated relationship can be successfully applied to actual radar imagery. To do this an image of the Howland study area was produced from the PHH and CHH AIRSAR data. This image data was analyzed in an earlier article by Ranson and Sun (1994), which determined that the best band combination for estimating biomass in the study area was the combination of PHV and CVH [i.e., PHV–CHV (dB)]. Therefore, we use the results of this earlier work as the basis for evaluating the algorithms described above.

The equation reported by Ranson and Sun (1994) was used to estimate biomass from the PHV–CHV AIRSAR image. Briefly, average biomass was determined from a 5×5 array of mapped biomass pixels for each of the 49 measurement locations. The averaged values were compared with the measured biomass by determining the best-fit line through the paired observations. Figure 8 compares the biomass from the AIRSAR image and field measured biomass data. The resulting equation was

$$\text{Biomass}_{(\text{image})} = 3.633 + 0.630\ \text{Biomass}_{(\text{field})}, \qquad r^2 = 0.76. \tag{6}$$

The use of PHV–CHV was reported by Ranson and Sun to have better sensitivity than any other single band or combination of bands used in their study. Examination of the predicted vs. observed data using AIRSAR PHH–CHH data and Eq. (4) reveals an apparent lack of sensitivity to biomass greater than about 15 kg/m^2 (Fig. 7b) and an overall underestimation of the biomass in the study area.

Figure 9 illustrates the relationship between the biomass predicted using the calibrated model backscatter [Eq. (5)] and measured biomass (dashed line). The apparent saturation for biomass above about 15 kg/m^2 is present in this figure as well. From Table 5 it can be seen that the results for all the model and data analyses

Table 5. Comparison of Model Performance with Observed Biomass from Field Measurements and Predicted Biomass Extracted from Biomass Image[a]

Biomass Range: 0–37 kg/m^2					
Model	*Source*	b_0	b_1	r^2	*RMSE (kg/m^2)*
Modeled biomass modeled PHH-CHH (uncalibrated)	Eq. (2)	6.603	0.374	0.526	6.523
Modeled biomass modeled PHH-CHH (calibrated)	Eq. (5)	5.052	0.447	0.526	6.567
Field biomass AIRSAR PHH-CHH	Eq. (4)	5.543	0.447	0.517	6.233
Field biomass AIRSAR PHV-CHV	Ranson and Sun (1994)	2.098	0.738	0.741	5.077

[a] Y predicted=b_0+b_1∘X observed.

Table 6. Same as Table 5 Except Limited Range of Biomass Was Used

Biomass Range: 0–15 kg / m²					
Model	*Source*	b_0	b_1	r^2	*RMSE (kg / m²)*
Modeled biomass modeled PHH-CHH (uncalibrated)	Eq. (2)	3.734	0.944	0.725	4.236
Modeled biomass modeled PHH-CHH (calibrated)	Eq. (5)	1.733	1.107	0.736	3.681
Field biomass AIRSAR PHH-CHH	Eq. (4)	1.999	1.180	0.735	4.313
Field biomass AIRSAR PHV-CHV	Ranson and Sun (1994)	1.394	0.757	0.650	3.055

are similar with the uncalibrated model results being the worst and the measurement-based PHV–CHV being the best (i.e., slope and intercept terms are closer to 0.0 and 1.0, respectively and the root mean square error is minimized).

The insensitivity to biomass above a certain value has been reported by several researchers. Depending on the type of SAR data used and the type forest studied, the upper value of biomass sensitivity reported has ranged from 10 kg / m² to 25 kg / m² (e.g., LeToan et al., 1992; Dobson et al., 1995). Based on the results presented in Figures 8 and 9 and Table 5, we limited the data to less than 15 kg / m² and reanalyzed the data. This improved the results as shown in Table 6. The slopes of the predicted versus measured regression lines are closer to 1.0, indicating a removal of the bias towards underestimating biomass seen in Table 5. Intercepts are still high, indicating the lower limit of biomass detection may be around 2–3 kg / m² for this analysis. RMSE also were reduced to less than 4.3 kg / m². Note that the results of applying the algorithm developed from the models and using calibrated data [Eq. (5)] is slightly better than using the AIRSAR PHH–CHH and field measurements derived algorithm [Eq. (4)].

Given the improved results in Table 6 a biomass image was prepared by classifying the AIRSAR image into four biomass levels: 0–5 kg / m², 5–10 kg / m², 0–15 kg / m², and greater than 15 kg / m². Figure 10a presents the total power composite image produced from the AIRSAR data. Roads, water, and clearing are obvious in the image as dark areas. Forest areas appear orange and yellow as a result of more scattering in P- and L-bands. There is an obvious incidence angle effect from top (larger incidence angle) to bottom (small incidence angle). Figure 10b is the biomas image produced from the AIRSAR data using Eq. (5) for the same area. The dark brown areas in the biomass image (Fig. 10b) correspond to areas devoid of vegetation such as roads and rivers and recently cleared forest. These latter areas are found mostly in the center and on the right side of the image. Low (green) levels of biomass can be found in clear cuts with substantial regrowth such as the large area in the upper left of the image. Moderate (yellow) and high (red) biomass densities are found in areas of heavier forest cover. The areas in Figure 10b with estimated biomass in the four categories were found to be: 0–5 kg / m²=9.7%, 5–10 kg / m²=25.2%, 10–15 kg / m²=40.8%, and 15 > kg / m²=24.3%. Of the 102,459 pixels coded as the highest biomass category, 89,658 pixels or nearly 88% were mapped between 15 kg / m² and 20 kg / m² biomass. This suggests that the biomass map may be a reasonable result for the biomass distribution in the study area with 95% of the area mapped to 20 kg / m² or less.

The combined modeling approach can be used to infer average rates of change as well as inventory biomass. The forest succession model shows different rates of biomass accumulation at different stages of stand development (viz., the slopes of the biomass trajectories in Fig. 4). Pooling simulations for the different soil types and stratifying by biomass, we estimated average annual rates of biomass accumulation for categories of biomass (see Table 7). Biomass accumulation rates for the lowest biomass category were determined for two levels: 0–1 kg / m² to represent recently disturbed stands and 1–5 kg / m² to represent established young stands. The highest rates of biomass increase (0.37 kg / m² / yr) were seen in these younger stands. Well-established stands of moderate (5–10 kg / m²) biomass accumulated biomass at a slower rate (0.17 kg / m² / yr). The highest biomass stands (> 10 kg / m²) were predicted to have very slow growth at only 0.02 kg / m² / yr. The results summarized in Table 7 indicate that the majority (65%) of the imaged study area is in relatively slowly growing, high biomass forest stands. This type of information is useful for understanding both current productivity levels and future trends of the forest's development. Note, however, that the lowest biomass categories could not be resolved separately and combine to form 9.7% of the forest area. Of this 9.7%, a small fraction is in nonforest such as roads, water, and

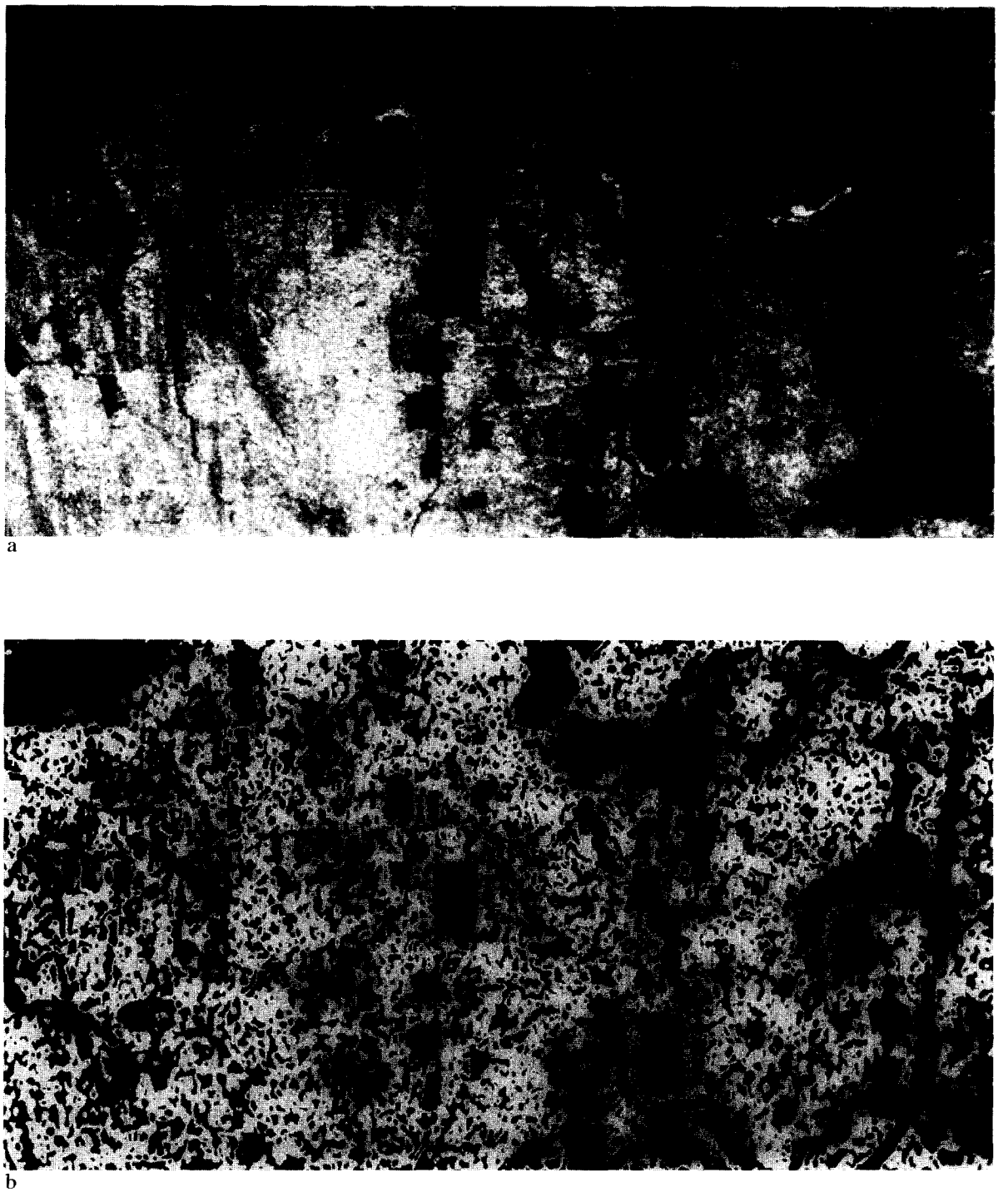

Figure 10. (a) Total power composite AIRSAR image for the NEF study site (P-band=red, L-band=green, C-band=blue). (b) Biomass image generated from model derived algorithm (Eq. 5). (0–5 kg/m^2=dark brown, 5–10 kg/m^2=green, 10–15 kg/m^2=yellow and > 15 kg/m^2=red). Images represent an area on the ground of about 11 km by 6 km. North is at top.

bare soil. While not a major source of error in our study site, an additional step of classifying the area into forest and nonforest categories would improve the results. The results will also be improved by the addition of species specific (i.e., broadleaf, needle leaf) growth rates and inclusion of other stand attributes such as leaf area index (e.g., Ranson et al., 1995b). These ideas will be addressed in future articles.

Table 7. Simulated Biomass Increment (kg m^{-2} y^{-1}) for Conifer Stands at the Northern Experimental Forest Classified into Biomass Categories

Biomass (kg/m^2)	*Low* (*0–1, 1–5*)	*Medium* (*5–10*)	*High* (*> 10*)
Biomass increment ($kg\ m^{-2}\ y^{-1}$)	0.17, 0.37	0.17	0.02
Percent of study area	9.7	25.2	65.1

SUMMARY AND CONCLUSIONS

This article has described a procedure to use a forest growth model, simulations of a northern forest in Maine, USA, to provide input parameters for a radar backscatter model. The results of the two models were used to develop a relationship between above ground biomass and radar backscatter. The model-derived relationship was found to underestimate biomass in an AIRSAR image and required calibration based on limited ground measurements. The combined modeling approach produced results consistent with those obtained from AIRSAR data and ground measurements when applied to image data and limited to biomass levels of 15 kg/m^2 or less.

The RMS errors of around 3.7 kg/m^2 are relatively high for biomass assessment purposes, but may be improved as the forest and backscatter models are improved. For example, the forest model uses the same functions for growth-dependent tree mortality across all species, which may not be appropriate for New England forests (Pacala *et al.*, 1996). It also uses a single function to relate foliage density and bole diameter for all species. More realistic dynamics might be provided by a model that explicitly follows carbon budgets of individual trees (Friend *et al.*, 1996), and a model that represents species differences in leaf area per sapwood area (Knox and Friend, 1996).

Other errors may have resulted from the use of a single incidence angle for the backscatter simulations. However, for dense canopies, PHH and CHH do not vary appreciably over the range of angles in the portion of the AIRSAR image used. There would be more variation for low bioomass stands where there is greater surface scattering. This effect is more important for aircraft SARs with a range of incidence angles across the image. The current radar model also does not simulate cross-polarized backscatter very well because of the lack of treatment of multiple scattering. This is an important limitation and will be addressed in future work.

The work presented in this article was performed at Goddard Space Flight Center and funded by NASA Headquarters Ecosystem Processes and Modeling Program RTOP 462-43 and SIR-C / XSAR Project RTOP 665-31. Dr. Weishampel's work was supported by the National Research Council while he was a resident at GSFC. Thanks to Professor Alan Strahler of Boston University for making the tree crown information available. Special thanks to International Paper for the use of their Northern Experimental Forest and the University of Maine for assistance in field measurements and logistics. The constructive criticisms of three anonymous reviewers are also appreciated.

REFERENCES

Bonan, G. B., and Hayden, B. P. (1990), Using a forest stand simulation model to examine the ecological and climatic significance of the late-Quaternary pine / spruce pollen zone in eastern Virginia, *Quart. Res.* 33:204–218.

Bonan, G. B., and Shugart, H. H. (1989), Environmental factors and ecological processes in boreal forests, *Annu. Rev. Ecol. Syst.* 20:1–2.

Bonan, G. B., Shugart, H. H., and Urban, D. L. (1990), The sensitivity of some high-latitude boreal forests to climatic parameters. *Clim. Change* 16:9–29.

Botkin, D. B. (1993), *Forest Dynamics: An Ecological Model*, Oxford University Press, New York.

Botkin, D. B., Janak, J. F., and Wallis, J. R. (1972), Rationale, limitations, and assumptions of a northeastern forest growth simulator. *IBM J. Res. Dev.* 16:101–116.

Chauhan, N. S., Lang, R. H., and Ranson, K. J. (1991), Radar modeling of a boreal forest. *IEEE Trans. Geosci. Remote Sens.* 29:627–638.

Dobson, M. C., Ulaby, F. T., Le Toan, T., Beaudoin, A., Kasischke, E. S., and Christensen, N. (1992), Dependence of radar backscatter on coniferous forest biomass. *IEEE Trans. Geosci. Remote Sens.* 30:412–415.

Dobson, M. C., et al. (1995), Estimation of forest biophysical characteristics in northern Michigan with SIR-C / XSAR, *IEEE Trans. Geosci. Remote Sens.* 33:877–895.

Doyle, T. W. (1981), The role of disturbance in the gap dynamics of a montane rain forest: an application of a tropical forest succession model, in *Forest succession: Concepts and Application* (D. C. West, H. H. Shugart, and D. B. Botkin, Eds.), Springer-Verlag, New York, pp. 56–73.

Durden, S. L., van Zyl, J. J., and Zebker, H. A. (1989), Modeling and observation of the radar polarization signature of forest areas. *IEEE Trans. Geosci. Remote Sens.* 27:290–301.

Frew, J. (1990), The image processing workbench, Ph.D. dissertation, Dept. of Geography, University of California–Santa Barbara. 306 pp.

Friend, A. D., Stevens, A. K., Knox, R. G., and Cannell, M. G. R. (1996), A process-based, terrestrial biosphere model of ecosystem dynamics (Hybrid 3.0). *Ecol. Model.* (in press).

Fung, A. K., and Pan, G. W. (1987), A scattering model for perfectly conducting random surface: I. Model development. *Int. J. Remote Sens.* 8:1579–1605.

Goward, S. N., Williams, D. L., and Peterson, D. L. (1994), NASA multisensor aircraft campaigns for the study of forest ecosystems. *Remote Sens. Environ.* 47:107–108.

Hall, F. G., Huemmrich, K. F., Strebel, D. E., Goetz, S. J., Nickeson, J. E., and Woods, K. D. (1992), Biophysical, morphological, canopy optical property, and productivity data from the Superior National Forest, NASA Technical Memorandum 104568, NASA / GSFC, Code 923, Greenbelt, MD 20771.

Hallikainen, M. T., Ulaby, F. T., Dobson, M. C., El-Rayes, M. A., and Wu, L.-K. (1985), Microwave dielectric behavior of wet soil—Part I: Empirical models and experimental observations. *IEEE Trans. Geosci. Remote Sens.* GE-23: 25–34.

Hinckley, T. M., et al. (1994), Use of the JABOWA family of individual-tree based models for exploration of forest responses to global climate change, Report, National Council on Air and Stream Improvement.

Karam, M. A., Fung, A. K., Lang, R. H., and Chauhan, N. S. (1992), A microwave scattering model for layered vegetation. *IEEE Trans. Geosci. Remote Sens.* 30(4):767–784.

Kasischke, E. S., and Christensen, N. L. (1990), Connecting forest ecosystem and microwave backscatter models. *Int. J. Remote Sens.* 11:1277–1298.

Kimes, D. S., and Smith J. A. (1991), Inclination distributions and measurements of hemlock and red spruce needles. *Appl. Opt.* 3036:5226–5228.

Knox, R. G., and Friend, A. D. (1996), Vegetation dynamics from physiological and functional principles and a resulting paradox in mechanistic reduction, forthcoming.

Lang, R. H., Landry, R., Kavaklioglu, O., and Deguise, J. C., (1994), Simulation of microwave backscatter from a red pine stand, in *Multispectral and Microwave Sensing of Forestry, Hydrology, and Natural Resources* (E. Mougin, K. J. Ranson, and J. Smith, Eds.), Proc. Europta Series, SPIE Vol. 2314, 26–30 September, pp. 2314–2316.

Le Toan, T., Beaudoin, A., Riom, J., and Guyon, D. (1992), Relating forest biomass to SAR data. *IEEE Trans. Geosci. Remote Sens.* 30:403–411.

Levine, E. R., Ranson, K. J., Smith, J. A., et al. (1993), Forest ecosystem dynamics: linking forest succession, soil process and radiation models. *Ecol. Model.* 65:199–219.

Levine, E. R., Knox, R. G., and Lawrence, W. (1994), Relationships between soil properties and vegetation at the Northern Experimental Forest, Howland, Maine. *Remote Sens. Environ.* 47:231–241.

Levine, E. R., Knox, R. G., and Hammond, K. (1995), Modeling soil and snow dynamics in northern forests: preliminary results, in *Proc. American Geophysical Union Annual Meeting*, Baltimore, MD.

MathSoft (1993), *S-Plus Guide to Statistical and Mathematical Analysis*, Version 3.2.

McDonald, K. C., and Ulaby, F. T. (1993), Radiative transfer modeling of discontinuous tree canopies at microwave frequencies. *Int. J. Remote Sens.* 14:2097–2128.

Pacala, S. W., Canham, C. D., Saponara, J., Silander, J. A., Kobe, R. K., and Ribbens, E. (1996), Forest models defined by field measurements: estimation, error analysis and dynamics, *Ecol. Monogr.* 66:1–43.

Pastor, J., and Post, W. M. (1985), Development of a linked forest productivity-soil process model, ORNL/TM-9519, Oak Ridge National Laboratory, Oak Ridge, TN.

Pastor, J., and Post, W. M. (1988), Response of northern forests to CO_2 induced climate change, *Nature* 334:55–58.

Pearlstine, L., McKellar, H., and Kitchens, W. (1985), Modeling the impacts of river diversion on bottomland forest communities in the Santee River floodplain, South Carolina. *Ecol. Model.* 29:283–302.

Pierce, L. E., Sarabandi, K., and Ulaby, F. T. (1994), Application of an artificial neural network in canopy scattering inversion. *Int. J. Remote Sens.* 15:3263–3270.

Polatin, P. F., Sarabandi, K., and Ulaby, F. T. (1994), An iterative inversion algorithm with application to the polarimetric radar response of vegetation canopies. *IEEE Trans. Geosci. Remote Sens.* 32:62–70.

Ranson, K. J., and Sun, G. (1994), Mapping biomass for a northern forest using multifrequency SAR data. *IEEE Trans. Geosci. Remote Sens.* 32:388–396.

Ranson, J. J. and Sun, G. (1996), An evaluation of AIRSAR and SIR-C/XSAR images of northern forest attributes in Maine, USA. *Remote Sens. Environ.* (in press).

Ranson, K. J., Sun, G., Weishampel, J. F., and Knox, R. G. (1994), Interfacing forest succession and remote sensing models for forest ecosystem studies in *Multispectral and Microwave Sensing of Forestry, Hydrology, and Natural Resources* (E. Mougin, K. J. Ranson, and J. Smith, Proc. Europta Series, SPIE Vol. 2314, 26–30 September, pp. 526–537.

Ranson, K. J., Saatchi, S., and Sun, G. (1995a), Boreal forest ecosystem characterization with SIR-C/XSAR, *IEEE Trans. Geosci. Remote Sens.* 33:867–876.

Ranson, K. J., Smith, J. A., Sun, G., Weishampel, J. F., and Knox, R. G. (1995b), Forest structure from combined optical and microwave modeling and measurements, in *Proc. Combined Optical-Microwave Earth and Atmosphere Sensing (CO-Meas '95)*, Atlanta, GA.

Richards, J. A., Sun, G., and Simonett, D. S. (1987), L-band radar backscatter modeling of forest stands, *IEEE Trans. Geosci. Remote Sens.* GE-25:487–498.

Rignot, E., Way, J., Williams, C., and Viereck, L. (1994), Radar estimates of above ground biomass in boreal forests of interior Alaska. *IEEE Trans. Geosci. Remote Sens.* 32:1117–1124.

Saatchi, S., and Moghaddam, M. (1994), Biomass distribution in boreal forest using SAR imagery, in *Multispectral and Microwave Sensing of Forestry, Hydrology, and Natural Resources* (E. Mougin, K. J. Ranson, and J. Smith, Eds.), Proc. Europta Series, SPIE Vol. 2314, 26–30 September, pp. 437–448.

Shugart, H. H., Hopkins, M. S., Burgess, I. P., and Mortlock, A. T. (1980), The development of a succession model for subtropical rain forest and its application to assess the effects of timber harvest at Wiangaree State Forest, *N. S. W. J. Environ. Manage.* 11:243–265.

Shugart, H. H., Smith, T. M., and Post, W. M. (1992), The potential for application of individual-based simulation models for assessing the effects of global change. *Annu. Rev. Ecol. Syst.* 23:15–38.

Smith, J. A., Ranson, K. J., Shimabakuro, Y. E., et al. (1994), Evaluation of a multi-story, forest canopy remote sensing model driven by stand-level architecture, in *Multispectral and Microwave Sensing of Forestry, Hydrology, and Natural Resources* (E. Mougin, K. J. Ranson, and J. Smith, Eds.), Proc. Europta Series, SPIE Vol. 2314, 26–30 September, pp. 2–8.

Strahler, A. (1995), Personal communication, Boston University, Boston, MA 02215.

Sun, G., and Ranson, K. J. (1995), A three-dimensional radar backscatter model of forest canopies, *IEEE Trans. Geosci. Remote Sens.* 33:372–382.

Sun, G., Simonett, D. S., and Strahler, A. H. (1991), A radar backscatter model for a discontinuous coniferous forest. *IEEE Trans. Geosci. Remote Sens.* 29:639–650.

Ulaby, F. T., and El-Rayes, M. A. (1987), Microwave dielectric spectrum of vegetation, Part II: Dual-dispersion model, *IEEE Trans. Geosci. Remote Sens.* GE-25:550–557.

Ulaby, F., Sarabandi, K., McDonald, K., Whitt, M., and Dobson, M. (1990), Michigan Microwave Canopy Scattering Model (MIMICS), *Int. J. Remote Sens.* 11:1123–1253.

Urban, D. L. (1990), *A Versatile Model To Simulate Forest Pattern: A Users Guide to ZELIG,* Version 1.0, Environmental Sciences Department, University of Virginia, Charlottesville, VA 22903.

USDA (1990), Soil Survey and Interpretations of Selected Lands in Maine, USDA, SCS, Orono, ME.

Wang, Y., Day, J. L., and Sun, G. (1993), Santa Barbara microwave backscatter canopy model for woodlands. *Int. J. Remote Sens.* 14:1477–1493.

Weishampel, J. F., Knox, R. G., and Levine, E. R. (1996), Modeling soil saturation effects on forestdynamics across a southern boreal landscape, *Bull. Ecol. Soc. Am.*, forthcoming.

Wenger, K. F., Ed. (1984), *Forestry Handbook, 2nd Ed.*, Wiley, New York, 582 pp.

Whitt, M. W., and Ulaby, F. T. (1994), Radar response of periodic vegetation canopies. *Int. J. Remote Sens.* 15:1813–1845.

Young, H. E., Ribe, J. H., and Wainwright, K. (1980), *Weight tables for tree and shrub species in Maine.* Miscellaneous Report 230, Life Sciences and Agriculture Experiment Station, University of Maine at Orono, September.